

Journal Pre-proofs

Superior inhibition of influenza virus hemagglutinin-mediated fusion by indole-substituted spirothiazolidinones

Gökçe Cihan-Üstündağ, Muhammet Zopun, Evelien Vanderlinden, Elif Ozkirimli, Leentje Persoons, Gültaze Çapan, Lieve Naesens

PII: S0968-0896(19)31025-9
DOI: <https://doi.org/10.1016/j.bmc.2019.115130>
Reference: BMC 115130

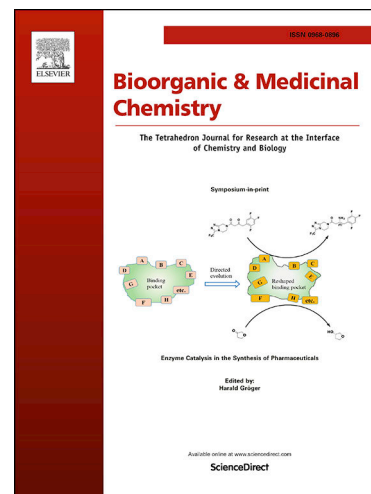
To appear in: *Bioorganic & Medicinal Chemistry*

Received Date: 22 June 2019
Revised Date: 12 September 2019
Accepted Date: 18 September 2019

Please cite this article as: G. Cihan-Üstündağ, M. Zopun, E. Vanderlinden, E. Ozkirimli, L. Persoons, G. Çapan, L. Naesens, Superior inhibition of influenza virus hemagglutinin-mediated fusion by indole-substituted spirothiazolidinones, *Bioorganic & Medicinal Chemistry* (2019), doi: <https://doi.org/10.1016/j.bmc.2019.115130>

This is a PDF file of an article that has undergone enhancements after acceptance, such as the addition of a cover page and metadata, and formatting for readability, but it is not yet the definitive version of record. This version will undergo additional copyediting, typesetting and review before it is published in its final form, but we are providing this version to give early visibility of the article. Please note that, during the production process, errors may be discovered which could affect the content, and all legal disclaimers that apply to the journal pertain.

© 2019 Elsevier Ltd. All rights reserved.



Graphical Abstract

To create your abstract, type over the instructions in the template box below.
Fonts or abstract dimensions should not be changed or altered.

Superior inhibition of influenza virus hemagglutinin-mediated fusion by indole- substituted spirothiazolidinones

Leave this area blank for abstract info.

Gökçe Cihan-Üstündağ^a, Muhammet Zopun^a, Evelien Vanderlinden^b, Elif Ozkirimli^c, Leentje Persoons^b,
Gültaze Çapan^a and Lieve Naesens^{b*}

^a*Department of Pharmaceutical Chemistry, Faculty of Pharmacy, Istanbul University, Istanbul 34116, Turkey*

^b*Rega Institute for Medical Research, KU Leuven, Department of Microbiology, Immunology and Transplantation, B-3000 Leuven, Belgium*

^c*Chemical Engineering Department, Bogazici University, Istanbul 34342 Turkey*



Superior inhibition of influenza virus hemagglutinin-mediated fusion by indole-substituted spirothiazolidinones

Gökçe Cihan-Üstündağ^a, Muhammet Zopun^a, Evelien Vanderlinden^b, Elif Ozkirimli^c, Leentje Persoons^b, Gültaze Çapan^a and Lieve Naesens^{b*}

^aDepartment of Pharmaceutical Chemistry, Faculty of Pharmacy, Istanbul University, Istanbul 34116, Turkey

^bRega Institute for Medical Research, KU Leuven, Department of Microbiology, Immunology and Transplantation, B-3000 Leuven, Belgium

^cChemical Engineering Department, Bogazici University, Istanbul 34342 Turkey

ARTICLE INFO

Article history:

Received

Received in revised form

Accepted

Available online

Keywords:

Indole

Spirothiazolidinone

Influenza virus

Hemagglutinin

Fusion

Antiviral

Inhibitor

In silico

ABSTRACT

The influenza virus hemagglutinin (HA) mediates membrane fusion after viral entry by endocytosis. The fusion process requires drastic low pH-induced HA refolding and is prevented by arbidol and tert-butylhydroquinone (TBHQ). We here report a class of superior inhibitors with indole-substituted spirothiazolidinone structure. The most active analogue **5f** has an EC₅₀ value against influenza A/H3N2 virus of 1 nM and selectivity index of almost 2000. Resistance data and *in silico* modeling indicate that **5f** combines optimized fitting in the TBHQ/arbidol HA binding pocket with a capability for endosomal accumulation. Both criteria appear relevant to achieve superior inhibitors of HA-mediated fusion.

2009 Elsevier Ltd. All rights reserved.

* Corresponding author. Tel.: +32-16-322098; e-mail: lieve.naesens@kuleuven.be

Journal Pre-proofs

Seasonal influenza is a major public health problem caused by globally circulating influenza A and B viruses. Serious complications are common in fragile persons such as infants, elderly or chronically ill individuals.¹ Besides, novel influenza A viruses can emerge from zoonotic reservoirs and cause severe pandemics such as occurred in 2009 (pH1N1) and at three occasions in the 20th century, namely in 1918 (Spanish influenza, H1N1), 1957 (H2N2) and 1968 (H3N2).² Two avian subtypes that are causing severe infections in humans, i.e. H5N1 and H7N9, are feared for their potential to evolve into a human-transmissible virus. The annual vaccination against seasonal influenza is only partially effective and prone to antigenic mismatch.³ In the past years, vaccine effectiveness was particularly low for the H3N2 subtype⁴, which also tends to cause more severe disease compared to pH1N1.⁵

The influenza A virus subtype is determined by two antigens embedded in the viral envelope: hemagglutinin (HA) and neuraminidase (NA). The clinical benefit of NA inhibitors (oseltamivir and zanamivir) was recently reviewed⁶, yet is threatened by potential drug resistance as was globally seen for oseltamivir in the period 2007-2009.⁷ Widespread resistance is particularly problematic for the M2 channel blockers (amantadine and rimantadine). Diverse antivirals are in the (pre)clinical pipeline^{8,9} and two polymerase inhibitors, favipiravir¹⁰ and baloxavir marboxil¹¹, were recently approved in a few countries.

A strategy preventing HA-mediated entry into host cells appears attractive to shut-off the viral and inflammatory cascades, yet is complicated by pronounced HA sequence variation. The eighteen HA subtypes are classified in two groups. The above-mentioned H1, H2 and H5 HAs fall in group 1 whereas the H3 and H7 HAs belong to group 2. The entry process starts with virus attachment, which requires recognition of sialylated cell surface glycans by the receptor binding domain in the globular head of HA.¹² After endocytic virus uptake followed by gradual endosome acidification from pH ~6 to pH ~5, the low pH induces drastic conformational rearrangements in HA. As a result, the hydrophobic fusion peptide leaves its buried position in the HA stem to provoke fusion of the viral and endosomal membranes.¹³ The fusion pore allows migration of the viral genome segments into the cytoplasm, followed by their nuclear import to initiate transcription and replication.^{14,15}

for more than two decades, with diverse scaffolds reported in the literature (reviewed in:¹⁵). More recently, several broadly neutralizing anti-HA antibodies (bnAbs) were found to interfere with HA-mediated fusion²¹, renewing also the relevance of small molecules to prevent this event. For example, one small molecule was rationally designed to optimally fit in the HA binding pocket of a group 1-specific bnAb.²² Thus far, arbidol (Fig. 1) is the only influenza virus fusion inhibitor that is commercially available in Russia (generic name: umifenovir) and China; it is under clinical evaluation in the USA.²³ Besides its inhibitory effect on HA-mediated fusion, arbidol exhibits a more general membrane-perturbing effect, explaining its broad activity against several viruses distinct from influenza virus.²⁴ A recent cocrystallographic study revealed the precise binding mode of arbidol within the stem region of H3 and H7 HAs.¹⁶ The arbidol binding pocket in H3 HA (Fig. 2) partially overlaps with that of tert-butyl hydroquinone (TBHQ; Fig. 1), a group 2-specific inhibitor.¹⁷ For other fusion inhibitors, the binding mode is less well defined although evidence was provided by virus resistance, HA interaction or *in silico* docking studies. Except for arbidol, all reported influenza virus fusion inhibitors display narrow activity against specific HA subtypes, which appears related to the size, accessibility or charge of their HA binding pocket. In this context, the “TBHQ pocket” appears particularly important, since it is the binding site for TBHQ and arbidol in H3 HA, and proposedly also for some aniline-based inhibitors with HA group 1 (H1 and H5) specificity.²⁵

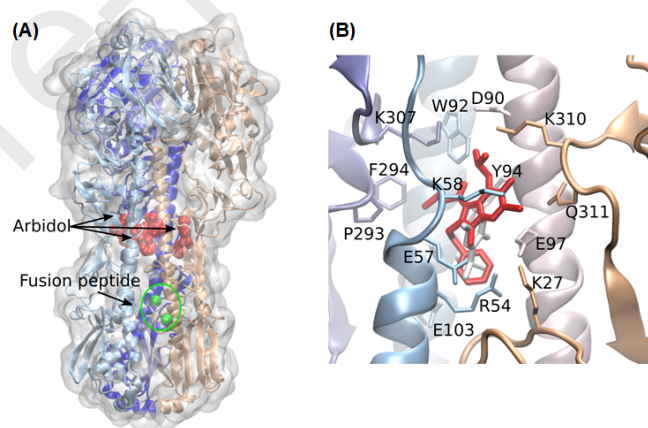


Figure 2. Reported HA binding mode for arbidol and TBHQ. (A) Binding site of arbidol in complex with trimeric H3 HA¹⁶, relative to location of the fusion peptide (of which the N-terminus is marked by a green sphere). The three HA protomers are shown in lavender, blue and beige ribbons. Each of the three arbidol molecules (red vdW spheres) binds at the interface between two protomers. (B) Binding mode of arbidol (in red) and TBHQ (in white) in reported crystal structures^{16,17}, showing their interactions with monomer 1 (HA1 in violet and HA2 in blue) and monomer 2 (HA1 in orange and HA2 in pink). The Figure presents the H3 HA protein and arbidol ligand in PDB entry 5T6N, onto which the binding pose of TBHQ (from PDB entry 3EYM) was superimposed.

We previously identified a class of influenza virus fusion inhibitors with *N*-(1-thia-4-azaspiro[4.5]decan-4-yl)carboxamide (spirothiazolidinone) scaffold and strong activity against H3 HA.¹⁸ The lead compound, **B1**, is shown in Fig. 1. Combined A/H3N2 resistance, biochemical and *in silico* docking experiments indicated that the spirothiazolidinone moiety binds to H3 HA in the same pocket as TBHQ.¹⁷ In addition, the imidazo[2,1-*b*]thiazole part of **B1** was predicted to form favorable hydrophobic interactions. Subsequent SAR analyses showed that this moiety could be replaced by 2-hydroxyphenyl (**B2**)¹⁸, 1-adamantyl (**B3**)¹⁹ or 5-chloro-2-hydroxyphenyl (**B4**)²⁰ (Fig. 1), although antiviral efficacy and selectivity were not drastically changed. In the

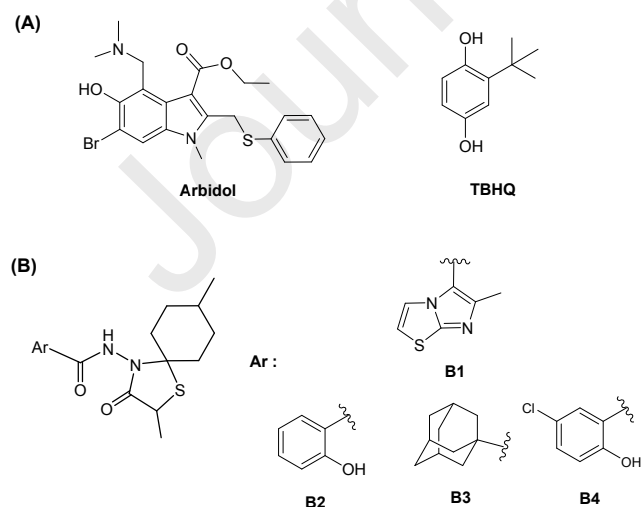


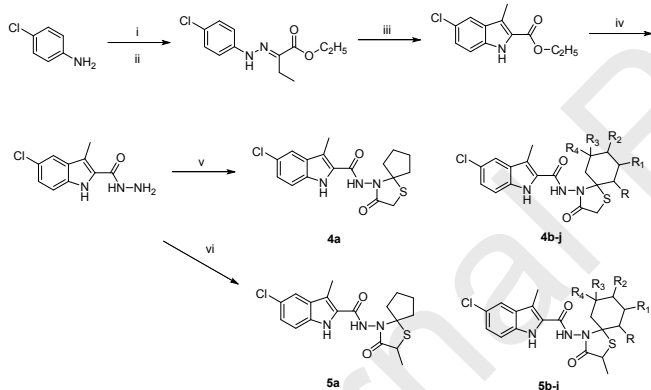
Figure 1. Chemical structures of influenza virus fusion inhibitors relevant for this study. (A) Arbidol and tert-butylhydroquinone (TBHQ) which have been cocrystallized with H3 HA^{16,17}; (B) H3 HA-specific spirothiazolidinone compounds discovered by our group and for which a few variations in the aryl (Ar) moiety were explored as indicated¹⁸⁻²⁰.

pres inhibition for a new and particularly potent series of analogues carrying an indole function. This core was found to offer an impressive 4000-fold gain in antiviral activity compared to the original lead **B1**. The best analogue, **5f**, displays nanomolar activity against influenza A/H3N2 virus and classifies as the most potent influenza virus fusion inhibitor ever described. Resistance data with mutant H3 HA proteins were rationalized by *in silico* docking, showing partial binding similarities between **5f** and arbidol or TBHQ. We propose that **5f** owes its superior anti-A/H3N2 activity to optimal interactions with H3 HA, combined with a capability for endosomal accumulation.

2. Results and discussion

2.1. Chemical synthesis and structural characterization

The synthetic pathways for spirothiazolidinones **4a-j** and **5a-j** are shown in Scheme 1. The diazonium salt, obtained from 4-chloroaniline and NaNO₂ plus HCl, was reacted with ethyl 2-ethyl-3-oxobutanoate to achieve compound **1** according to the Japp-Klingemann reaction. The Fischer indole synthesis was carried out in acidic media to cyclize **1** into ethyl 5-chloro-3-methyl-1*H*-indole-2-carboxylate (**2**). Subsequent exposure of **2** to an excess of hydrazine hydrate afforded compound **3**.²⁶ The target spirocyclic compounds (**4a-j**, **5a-j**) were synthesized by treatment of the key intermediate **3** with an appropriate cyclic ketone and mercapto acids in a one-pot reaction.²⁷



Scheme 1. Synthesis of 4a-j and 5a-j. Reagents and conditions: (i) 7% NaNO₂, EtOH, conc. HCl, 0 °C; (ii) ethyl 2-ethyl-3-oxo-butanoate, KOH, EtOH, 0 °C; (iii) conc. HCl, reflux, 4h; (iv) H₂NNH₂·H₂O, EtOH, reflux, 6h; (v) cyclopentanone/4-(non)substituted cyclohexanone, mercaptoacetic acid, dry toluene, reflux, 5–6 h; (vi) cyclopentanone/4-(non)substituted cyclohexanone, 2-mercaptopropionic acid, dry toluene, reflux, 5-6 h. Compounds: **4b**, **5b**: R,R₁,R₂,R₃,R₄=H; **4c**, **5c**: R=CH₃; R₁,R₂,R₃,R₄=H; **4d**, **5d**: R₁=CH₃; R₂,R₃,R₄=H; **4e**, **5e**: R₂=CH₃; R₁,R₁,R₃,R₄=H; **4f**, **5f**: R₂=C₂H₅; R₁,R₁,R₃,R₄=H; **4g**, **5g**: R₂=C₃H₇; R₁,R₁,R₃,R₄=H; **4h**, **5h**: R₂=C(CH₃)₃; R₁,R₁,R₃,R₄=H; **4i**, **5i**: R₁,R₃,R₄=CH₃; R₂=H; **4j**, **5j**: R₂=C₆H₅; R₁,R₁,R₃,R₄=H.

The new compounds were characterized by combustion analysis, IR, ¹H-NMR, ¹³C-NMR (APT), 2D-NMR (HSQC, HMBC) and electrospray ionization mass spectrometry (ESI-MS). The shifts observed in the amide carbonyl bands (1645-1685 cm⁻¹) when compared to that of **3** (1606 cm⁻¹) and the presence of new lactam carbonyl absorptions (1692-1707 cm⁻¹) characteristic for 4-thiazolidinones in the IR spectra of **4**, **5** proved the aimed cyclization. The NH₂ resonance of the intermediate hydrazide (**3**) at δ 4.53 ppm disappeared in the ¹H-NMR spectra of **4** and **5** as the group participated in ring formation and new resonances assigned to the spirodecane system appeared in the δ 0.75-2.55 ppm region

spirodecane C2-H₂ protons of **4a-j** resonated at about δ 3.55-3.71 ppm as singlets (except for the spectrum of compound **4i** in which C2-H₂ protons were observed as separate doublets due to the geminal interaction) and C2-H protons of **5a-j** resonated at about δ 3.84-3.99 ppm as quartets. ¹³C-NMR (APT) experiments and two-dimensional HSQC and HMBC experiments allowed complete assignment of proton and carbon signals. Resonances at δ 162.19-163.58 ppm and δ 168.33-171.09 ppm regions were assigned to the indolecarboxamide carbonyl and spirocyclic lactam carbonyl groups, respectively. This assignment was substantiated by the cross peaks between the spirodecane C2-H, 2-CH₃ protons and lactam C=O carbon and the cross peak between the indole-3-CH₃ protons and indolecarboxamide C=O carbon in the HMBC spectrum of compound **5e**.

Deprotonated [M-H]⁻ or protonated [M+H]⁺ ions observed in the ESI-MS confirmed the molecular weight of the compounds. Additional [(M-H)+2]⁻ or [(M+H)+2]⁺ isotope peaks approximately one-third the intensity of the molecular ion peak were further observed because of the ³⁷Cl isotope.

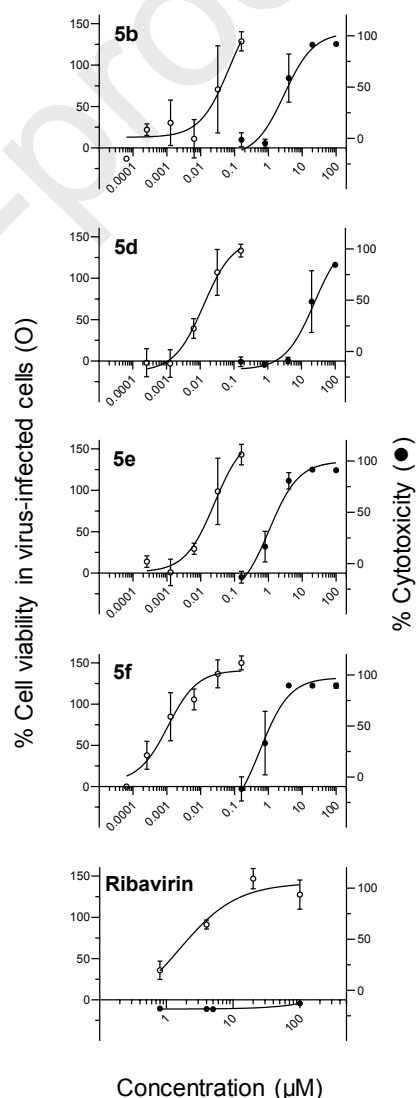


Figure 3. Dose-response curves. The graphs, generated with Graphpad Prism, show the dose-dependent inhibition of virus-induced CPE (O; left axis) versus cytotoxicity (●; right axis), both determined by MTS cell viability assay. Data points are the mean ± SEM (N=4).

Compound	R	R ₁	R ₂	R ₃	R ₄	EC ₅₀ ^b (μM) against influenza A/H3N2 virus		Cytotoxicity (μM)	
						CPE	MTS	MCC ^c	CC ₅₀ ^d
Analogues lacking the 2-methyl in the spiro ring									
4a	-	-	-	-	-	>100	>100	>100	>100
4b	H	H	H	H	H	>100	>100	>100	>100
4c	Me	H	H	H	H	>100	>100	≥20	>100
4d	H	Me	H	H	H	>100	>100	≥100	>100
4e	H	H	Me	H	H	>100	>100	≥100	>100
4f	H	H	Et	H	H	>100	>100	≥4	94
4g	H	H	Pr	H	H	>100	>100	0.8	1.3
4h	H	H	<i>t</i> -Bu	H	H	>100	>100	0.8	2.1
4i	H	Me	H	Me	Me	>100	>100	>100	>100
4j	H	H	Ph	H	H	>100	>100	5.0	2.4
Analogues carrying the 2-methyl in the spiro ring									
5a	-	-	-	-	-	>100	>100	>100	>100
5b	H	H	H	H	H	0.085 ± 0.041	0.063 ± 0.022 [92]	≥4	5.8
5c	Me	H	H	H	H	>100	>100	≥20	88
5d	H	Me	H	H	H	0.031 ± 0.023	0.023 ± 0.019 [1435]	≥4	33
5e	H	H	Me	H	H	0.063 ± 0.027	0.045 ± 0.014 [62]	0.87	2.8
5f	H	H	Et	H	H	0.0012 ± 0.0008	0.00077 ± 0.00023 [1948]	3.0	1.5
5g	H	H	Pr	H	H	>100	>100	0.8	1.9
5h	H	H	<i>t</i> -Bu	H	H	>100	>100	≥4	0.9
5i	H	Me	H	Me	Me	>100	>100	20	85
5j	H	H	Ph	H	H	>100	>100	1.0	2.3
B1	-	-	-	-	-	5.0 ± 2.3	3.2 ± 2.3 [>31]	≥100	>100
Ribavirin						8.4 ± 1.6	4.6 ± 3.2	≥100	>100
Amantadine						3.8 ± 0.2	1.2 ± 0.2	>200	>200

^a Madin-Darby canine kidney cells.

^b Antiviral EC₅₀ (mean ± SEM; N = 4): compound concentration producing 50% inhibition of virus-induced CPE, as determined by microscopy or by the MTS cell viability assay. The value in square brackets represents the selectivity index or ratio of CC₅₀ to EC₅₀ based on the MTS assay.

^c Minimum compound concentration that causes a microscopically detectable alteration of normal cell morphology.

^d 50% cytotoxic concentration based on the cell viability MTS assay.

2.2 SAR analysis for inhibition of influenza virus replication

The newly synthesized compounds were evaluated in Madin-Darby canine kidney (MDCK) cells infected with influenza A/H1N1, A/H3N2 or B virus. Antiviral activity was estimated from protection against virus-induced cytopathic effect (CPE) using microscopic scoring and MTS-based cell viability assay; both assays yielded very similar antiviral EC₅₀ values. These methods were also used to monitor compound cytotoxicity. Table 1 shows the clearly delineated SAR for inhibition of influenza A/H3N2 virus. There was no effect on influenza A/H1N1 or B virus (data not shown). The four compounds showing strong activity, i.e. **5b**, **5d**, **5e** and **5f**, all carry a methyl substituent at position 2- of the spirocyclic ring system; their counterparts lacking this moiety, i.e. **4b**, **4d**, **4e** and **4f**, were inactive (Table 1). The most active analogue **5f**, with an 8-ethyl function, had an antiviral EC₅₀ value as low as 1 nM and an impressive selectivity index (ratio of CC₅₀ to EC₅₀; both based on the MTS assay) of almost 2000. Its activity was 27-, 54- and 74-fold superior compared to the analogues bearing, respectively, a 7-methyl (**5d**), 8-methyl (**5e**) or no substituent (**5b**) on the spiro ring. Moving the methyl group to position 6- (**5c**) was deleterious. Also, a larger substituent at position 8- was not tolerated, i.e. in the compounds carrying a propyl (**5g**), tert-butyl (**5h**) or phenyl (**5j**). Compound **5a** bearing a spiro-fused cyclopentane ring (instead of cyclohexane) was also devoid of antiviral activity. The SAR of the indole-spirothiazolidinones nicely agrees with what we previously reported for the imidazo[2,1-*b*]thiazole; 2-hydroxyphenyl¹⁸; 1-adamantyl¹⁹; and 5-chloro-2-hydroxy-phenyl²⁰ series. Still, the indole moiety provided an impressive gain in anti-influenza virus activity since indole compound **5f** (antiviral EC₅₀: 1 nM) was 4000-fold more potent

than the corresponding imidazo[2,1-*b*]thiazole analogue (**B1**; EC₅₀: 4 μM).¹⁸

Several compounds were devoid of cytotoxicity at 100 μM (the highest concentration tested) (Table 1). For most other molecules, there was consensus between the cytotoxicity values obtained by the microscopic (MCC) or MTS (CC₅₀) assay. There was no correlation between antiviral and cytotoxic activity. For **5b**, **5d**, **5e** and **5f**, the superior activity and selectivity are evident from the dose-response curves shown in Fig. 3.

2.3. Inhibitory effect on HA-mediated membrane fusion

We next evaluated the compounds in the polykaryon assay, in which cell-cell fusion is monitored when influenza virus HA-expressing cells are briefly exposed to a buffer at pH 5. In cells transfected with wild-type (WT) H3 HA, very comparable EC₅₀ values were noted for the four indole derivatives tested, i.e. **5b**, **5d**, **5e** and **5f**, and their imidazo[2,1-*b*]thiazole analogue **B1** (Table 2). As evident from the dose-response curves in Fig. 4A, the spirothiazolidinone compounds had stronger inhibitory effect on polykaryon formation than TBHQ (~10-fold less active) and arbidol (~40-fold less active). We also tested activity against two mutant forms of H3 HA, which were previously identified when we passaged A/H3N2 virus in cell culture under selective pressure of **B1**.¹⁸ All five spirothiazolidinone molecules were highly impacted by HA mutations E57₂K and D112₂N (Table 2 and photographs in Fig. 4B). [Note: throughout the text, suffix 1 corresponds to residues from HA1 and suffix 2 to residues from HA2]. Resistance of the E57₂K mutant is explained by our model showing involvement of E57₂ in compound binding (see below). The E57₂K mutant HA was cross-resistant to the structurally distinct inhibitor

other substituted residue, D112₂, lies in the vicinity of the HA fusion peptide with which this aspartic acid residue is forming hydrogen bonds.²⁸ Mutation D112₂N was shown²⁹ to increase the fusion pH from 5.2 for WT-HA to 5.6 for the mutant (Table 2). This means that HA refolding occurs at higher pH, rendering the mutated protein insensitive to diverse fusion inhibitors, including TBHQ.^{17,30}

Table 2. Inhibitory effect in the polykaryon assay with WT or mutant^a forms of H3 HA.

Compound	EC ₅₀ ^b (μM)		
	HA-WT pH: 5.2 ^c	HA-E57 ₂ K pH: 5.2 ^c	HA-D112 ₂ N pH: 5.6 ^c
5b	1.3 ± 0.2	>25	>25
5d	1.4 ± 0.2	>25	>25
5e	2.1 ± 0.8	≥13	>25
5f	0.88 ± 0.15	>25	≥21
B1	1.1 ± 0.2	9.0 ± 2.6	>25
TBHQ	9.9 ± 0.4	12 ± 3	>400
Arbidol	40 ± 11	>200	>200

^a The two mutations in the HA2 subunit (E57₂K and D112₂N) were previously identified in influenza A/H3N2 viruses selected for resistance to imidazo[2,1-*b*]thiazole analogue **B1**.¹⁸ The mutations were introduced in an HA-expression plasmid to perform the polykaryon assay.

^b EC₅₀ (mean ± SEM; N = 3): compound concentration at which the number of polykaryons was 50% relative to the number observed in the no compound control.

^c Fusion pH (values reported in¹⁸): pH at which the number of polykaryons was 50% relative to the number seen at pH 4.9.

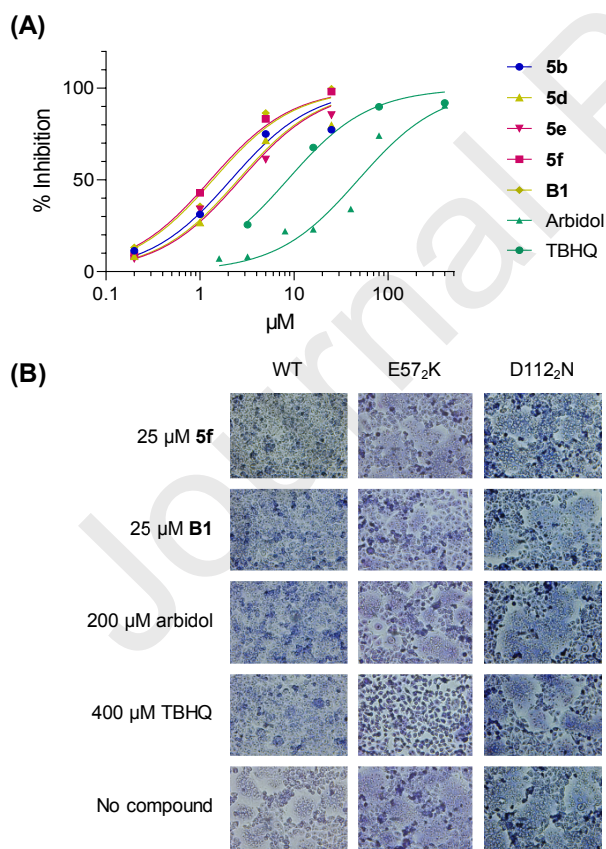


Figure 4. Inhibition in the HA polykaryon assay. (A) Dose-response curves for inhibition of wild-type (WT) H3 HA. Data points are the mean of three independent experiments. (B) The spirothiazolidinone compounds have no

photographs, original magnification 200x).

One striking observation was the marked potency shift between the HA-polykaryon assay and antiviral assay in MDCK cells. For indole compound **5f**, the difference between both assays was ~900-fold (= ratio between its EC₅₀ value against A/H3N2 virus in Table 1 and EC₅₀ value against WT-HA in Table 2). This shift is not explained by differences in the H3 HA protein sequences of A/HK/7/87 and A/X-31, used in the antiviral and polykaryon assays, respectively, since **5f** exhibited similar potency against both virus strains (EC₅₀ value in the CPE reduction assay: 7-fold lower for A/HK/7/87 compared to A/X-31; data not shown). The pronounced shift in EC₅₀ value between the antiviral assay and polykaryon assay was also seen with the other three indole compounds **5b**, **5d** and **5e**. In contrast, imidazo[2,1-*b*]thiazole compound **B1** displayed very similar EC₅₀ values in both assays. We hypothesize that the basic indole moiety in compound **5f** is protonated at low pH, leading to a positively charged indolium cation that may get trapped in the endosomes. A similar indolium ion trapping phenomenon is observed in pH-sensitive cyanine dyes.³¹ This plausibly results in high intra-endosomal compound concentrations for **5f** and amplification of its inhibitory effect on entering virus. For comparison, the imidazo[2,1-*b*]thiazole ring system in compound **B1** does not possess a basic nitrogen.

2.4 Molecular docking studies

In the TBHQ- (PDB ID: 3EYM) and arbidol- (PDB ID: 5T6N) bound crystal structures with H3 HA, the two ligands bind to the trimeric HA stem in an overlapping hydrophobic cavity situated at the interface between two protomers (Fig. 2A), with three ligand molecules bound per HA trimer. The inhibitors act as a glue to prevent the conformational rearrangement of HA required for membrane fusion. As noted previously¹⁶, the overall structural arrangement is quite similar in the two cocrystal structures and H3 HA apo form. Comparison of the arbidol and TBHQ cocrystal structures shows that the binding site residues also assume similar conformations, except for the R54₂ to N60₂ loop from monomer 1, which moves by about 1.5 Å RMSD, and E57₂ and K58₂ sidechains. These residues move away from the pocket to accommodate the larger arbidol molecule. In addition, the sidechain of K307₁ from monomer 1 points towards the amine group of arbidol while pointing away from the pocket in the TBHQ-bound structure.

The tert-butyl moiety of TBHQ (Fig 2B, ligand shown in white) makes hydrophobic interactions with residues I29₁, L98₂ and A101₂ of protomer 1, while the hydroquinone part pointed toward the solvent is surrounded by the charged residues R54₂ and E57₂ of protomer 1 and E97₂ of protomer 2. Arbidol (Fig. 2B, ligand shown in red) occupies the same hydrophobic pocket through its thiophenyl group, while its substituted indole ring occupies the pocket lined by E57₂ and K58₂ (protomer 1) and E97₂ (protomer 2). The indole makes hydrogen bonding and π -cation interactions with these residues as well as the aromatic residues W92₂ and F294₁ (both in protomer 1).

5f was docked into the two H3 HA structures (PDB ID: 3EYM and 5T6N) using an induced fit protocol that allows movement for ligand atoms and protein sidechain atoms surrounding the ligand. As expected given the resemblance between the two starting structures, the docked poses of **5f** were similar with comparable Glide Gscores of around -8 kcal/mol. In both cases the azaspiro group inserts into the hydrophobic pocket and the indole group is oriented towards the pocket mouth, which is lined by a network of ionizable residues. In the prediction (Fig. 5) starting from the arbidol-bound structure (PDB ID: 5T6N), the azaspiro group of **5f**

the same space as the thiophenyl group of arbidol and the thiazolidine ring of **5f** reaching out to interact with F294₁ of monomer 1 similar to the ester moiety of arbidol. Fig. 5A shows a comparison of arbidol (red) and **5f** (magenta) binding. The indole groups of **5f** and arbidol both point towards the solvent and make electrostatic interactions with the charged residues lining the pocket, such as E57₂ of monomer 1, which interacts with the positively charged indole nitrogen. When the TBHQ-bound structure was used, a similar binding pose was predicted for the spirolactam group of **5f**, while the indole plane was slightly rotated to position its positively charged nitrogen toward E97₂ of monomer 2 and its carbonyl substituent towards R54₂ and K58₂ of monomer 1. In both poses, an electrostatic network of interactions surrounded the indole moiety and it was stabilized by the presence of the positively charged indole nitrogen, suggesting that these consistently observed interactions are valid.

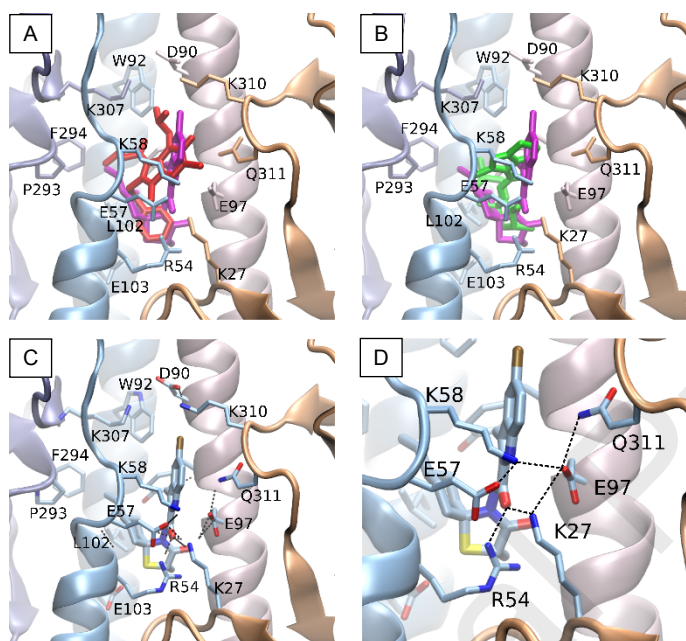


Figure 5. Predicted HA binding mode of **5f** and **B1**. The molecules were docked in the arbidol-H3 HA cocystal structure (PDB entry: 5T6N) between monomer 1 (chain C and D) and monomer 2 (chain E and F). (A, B) Overlay of **5f** (magenta) versus arbidol (red; panel A) or **B1** (green; panel B). The protein residues are colored according to HA chain (monomer 1: HA1 in violet and HA2 in blue; monomer 2: HA1 in orange and HA2 in pink). (C) Interaction network between **5f** and surrounding residues; H-bonds are shown as dashed lines. (D) Rationale for the E57K resistance mutation. E57₂ forms H-bonds with the carboxamide and indole moiety of **5f**.

The same docking exercise with **B1** into the arbidol-bound structure (Fig. 5B, green) predicted that the spiro moiety is again buried within the hydrophobic pocket while the imidazo[2,1-*b*]thiazole group faces the pocket mouth. Since this group lacks a positively charged nitrogen, it does not make interactions with E57₂ of monomer 1. However, the electrostatic network that surrounds the indole of arbidol and **5f** is also present around **B1**. The electrostatic bridge that forms between E97₂ of monomer 2 and K58₂ of monomer 1 was previously recognized to enhance the stability of the HA trimer.¹⁷ The network of interactions formed by these ionizable residues is stabilized by the carboxamide group present in both **5f** and **B1** (Fig. 5B, magenta and green). This may explain why, in the polykaryon experiments (see above), the two compounds have comparable activity towards H3 HA-mediated fusion. The docking results further clarify two aspects of the SAR

interactions with the target protein²⁴, namely (i) the absolute requirement for the thiazolidine methyl substituent at position 2 of the spirocyclic ring system that interacts with L98₂ and L102₂ in the hydrophobic pocket of protomer 1, and (ii) the favorable small alkyl substituent at position 8 of the cyclohexane ring, which makes hydrophobic contacts with P293₁ and F294₁ of protomer 1 (Fig. 5C). Hydrophobic interactions with L98₂ and L102₂ were shown to be critical for the binding of TBHQ¹⁷ and the cyclohexyl group of N-cyclohexyltaurine³³. Arbidol has also been reported to make CH- π interactions with F294₁ of monomer 1.¹⁶

Finally, the structural models offer an explanation for resistance of the E57₂K-mutant H3 HA protein, as demonstrated in the polykaryon experiments. Substitution of E57₂ by a lysine would introduce an extra positive charge very close to R54₂ and K58₂ of the aforementioned electrostatic network (Fig. 5D). Because these residues are solvent exposed, mutation E57₂K is tolerated by the protein and does not change the fusion pH. However, the mutant HA is resistant to arbidol and the spirothiazolidinones **5f** and **B1**. The resistance factor proved to be higher for **5f** than **B1**, since the ratio in EC₅₀ values for mutant versus WT was >28 for **5f** and 8 for **B1** (Table 2). While both compounds have a carboxamide moiety, **5f** (like arbidol) has an indole nitrogen that makes direct hydrogen bonding interactions with E57₂ of monomer 1, which would be lost upon substitution by lysine. Mutation E57₂K does not cause resistance to TBHQ. In the H3 HA trimer complexed with TBHQ, E57₂ adopts different orientations in the three ligand binding pockets¹⁷, suggesting that the presence of TBHQ does not stabilize the local interactions engaged by E57₂. Our biological data with E57₂K mutant HA nicely support the binding mode of our fusion inhibitors and of arbidol. This was not the case for resistance mutations detected in a previous study on arbidol, since these were located at regions remote from the arbidol binding pocket identified by X-ray studies.^{16,34}

3. Conclusion

We report a class of indole-substituted spirothiazolidinone inhibitors of HA-mediated fusion with unprecedented nanomolar activity against influenza A/H3N2 virus. The pronounced potency shift between the HA polykaryon versus antiviral assay indicates that the indole substituent in these inhibitors might lead to endosomal accumulation, a favorable characteristic that has not been recognized with fusion inhibitors before. Our inhibitors proved inactive against E57₂K-mutant HA protein, consistent with *in silico* predictions of their HA binding mode. While having an overlapping binding pocket with the known fusion inhibitors TBHQ and arbidol, the indole-substituted spirothiazolidinones have far higher inhibitory activity with obvious relevance for antiviral drug development.

4. Experimental section

4.1. Chemistry

4.1.1. General methods

Melting points were determined in open capillary tubes with a Buchi B-540 melting point apparatus and are uncorrected. Microanalyses were performed on a Thermo Finnigan Flash EA 1112 elemental analyzer. IR spectra were recorded in KBr discs (ν_{\max} in cm⁻¹) on a Shimadzu IRAffinity-1 FTIR spectrophotometer. ¹H-NMR (DMSO-*d*₆), ¹³C-NMR (APT) (DMSO-*d*₆) and heteronuclear correlation ¹H-¹³C (HSQC, HMBC) (DMSO-*d*₆)

Chemical shifts are reported as δ (ppm) relative to TMS as internal standard and coupling constants (J) are given in hertz (Hz). MS (ESI+/-) were determined on a Finnigan LCQ Advantage Max mass spectrometer (*: broad/distorted, ind.:indole, ar.:aromatic, sp.: spirodecane).

4.1.2. Ethyl 2-[2-(4-chlorophenyl)hydrazinylidene]butanoate (1)

To a solution of 4-chloroaniline (0.02 mol) in ethanol (10 mL), water (10 mL) and conc. HCl (6mL), 7% aqueous NaNO₂ solution (30mL) was added dropwise at 0 °C with stirring. The resulting solution of diazonium salt was poured into a cooled (0 °C) mixture of ethyl 2-ethyl-3-oxobutanoate (0.02 mol), ethanol (10 mL), water (10 mL), and KOH (5.4 g) while stirring. The resulting mixture was refrigerated overnight. The red oily solid residue thus obtained was separated, washed with water, and used without further purification.

4.1.3. Ethyl 5-chloro-3-methyl-1H-indole-2-carboxylate (2)

A solution of **1** (0.02 mol) in conc. HCl (20 mL) was heated under reflux on water bath (70-80 °C) for 4 h. The crude product was filtered off, washed with water until tested neutral to litmus and used without further purification.

4.1.4. 5-Chloro-3-methyl-1H-indole-2-carbohydrazide (3)²⁶

A mixture of **2** (0.02 mol), ethanol (20 mL) and H₂NNH₂.H₂O (98%, 8 mL) was heated under reflux on a water bath (70-80 °C) for 6 h. The resulting yellowish-brown solid was filtered off and recrystallized from ethanol. Mp 271-272 °C; IR(KBr): ν_{\max} 3296 (N-H), 1606 (C=O); ¹H-NMR (DMSO-d₆/500MHz): δ 2.44 (3H, s, 3-CH₃), 4.53 (2H, s, NH₂), 7.18 (1H, dd, J=8.8, 2.0 Hz, H6), 7.38 (1H, d, J=8.8 Hz, H7), 7.63 (1H, d, J=2.4 Hz, H4), 9.19 (1H, s, CONH), 11.32 (1H, s, NH).

4.1.5. General procedure for the synthesis of 5-chloro-3-methyl-N-(2,6,7,8,9-(non)substituted-3-oxo-1-thia-4-azaspiro[4.4]nonan/decan-4-yl)-1H-indole-2-carboxamides (4a-4j, 5a-5j)

A mixture of **3** (0.0025 mol), an appropriate cyclohexanone/cyclopentanone (0.003 mol) and mercaptoacetic acid or 2-mercaptopropionic acid (0.01 mol) was refluxed in 20 mL dry toluene for 5–6 h (150-200 °C) using a Dean-Stark water separator. Excess toluene was evaporated in vacuo. The resulting residue was triturated with saturated NaHCO₃ solution until CO₂ evolution ceased and was allowed to stand overnight or in some cases refrigerated until solidification. The solid thus obtained was washed with water, dried, and recrystallized from ethanol or ethanol–water.

4.1.6. 5-Chloro-3-methyl-N-(3-oxo-1-thia-4-azaspiro[4.4]nonan-4-yl)-1H-indole-2-carboxamide (4a)

White powder (55.0%); mp 269-272 °C; IR(KBr): ν_{\max} 3304 (N-H), 1697, 1651 (C=O); ¹H-NMR (DMSO-d₆/500MHz): δ 1.65-1.73 (4H, m, CH₂-sp.), 1.89-1.93 (2H, m, CH₂-sp.), 2.20 (2H, s*, CH₂-sp.), 2.49-2.51 (6H, m, 3-CH₃-ind., DMSO-d₆), 3.71 (2H, s, C2-H₂-sp.), 7.23 (1H, dd, J=8.7, 1.9, H6-ind.), 7.43 (1H, d, J=8.7, H7-ind.), 7.70 (1H, d, J=1.9, H4-ind.), 10.15 (1H, s, CONH), 11.49 (1H, s, NH); ¹³C-NMR (APT) (DMSO-d₆/125 MHz): δ 10.36, 10.43 (3-CH₃-ind.), 23.36, 29.41, 29.51, 29.61, 38.92 (CH₂-sp.), 76.45 (C5-sp.), 114.43, 114.53 (C7-ind.), 115.41 (C3-ind.), 119.95, 119.99 (C4-ind.), 124.69 (C5-ind.), 125.00, 125.12 (C6-ind.), 127.82 (C2-ind.), 129.52 (C3a-ind.), 135.00 (C7a-ind.), 162.28 (CO-NH), 168.36 (CO-sp.). MS (ESI-) m/z (%): 362.2 ([M-H]⁻, 100), 364.2 ([M-H+2]⁻, 29.9). Anal. Calcd for C₁₇H₁₈ClN₃O₂S (363.86): C, 56.12; H, 4.99; N, 11.55. Found: C, 56.25; H, 5.03; N, 11.33.

4.1.7. 5-Chloro-3-methyl-N-(3-oxo-1-thia-4-azaspiro[4.5]decan-4-yl)-1H-indole-2-carboxamide (4b)

3159 (N-H), 1707, 1654 (C=O); ¹H-NMR (DMSO-d₆/500 MHz): δ 1.00-1.12 (1H, m, CH₂-sp.), 1.42-1.50 (2H, m, CH₂-sp.), 1.58 (1H, d*, J=13.1, CH₂-sp.), 1.75 (2H, d*, J=13.5, CH₂-sp.), 1.80-1.90 (4H, s*, CH₂-sp.), 2.48-2.52 (5H, m, 3-CH₃-ind., DMSO-d₆), 3.64 (2H, s, C2-H₂-sp.), 7.24 (1H, dd, J=8.5, 1.9, H6-ind.), 7.43 (1H, d, J=8.3, H7-ind.), 7.70 (1H, d, J=1.9, H4-ind.), 10.10 (1H, s, CONH), 11.50 (1H, s, NH); ¹³C-NMR (APT) (DMSO-d₆/125 MHz): δ 10.39, 10.46 (3-CH₃-ind.), 23.61, 24.78, 28.62, 28.71, 37.82 (CH₂-sp.), 72.91 (C5-sp.), 114.41, 114.51 (C7-ind.), 115.54 (C3-ind.), 119.93, 119.97 (C4-ind.), 124.67 (C5-ind.), 124.97, 125.08 (C6-ind.), 127.86 (C2-ind.), 129.53 (C3a-ind.), 134.92 (C7a-ind.), 162.25 (CO-NH), 168.39 (CO-sp.). MS (ESI-) m/z (%): 376.1 ([M-H]⁻, 100), 378.1 ([M-H+2]⁻, 37.7). Anal. Calcd for C₁₈H₂₀ClN₃O₂S (377.88): C, 57.21; H, 5.33; N, 11.12. Found: C, 57.23; H, 5.20; N, 11.21.

4.1.8. 5-Chloro-3-methyl-N-(6-methyl-3-oxo-1-thia-4-azaspiro[4.5]decan-4-yl)-1H-indole-2-carboxamide (4c)

Beige crystals (51.3%); mp 270-272 °C; IR(KBr): ν_{\max} 3327, 3240 (N-H), 1697, 1670 (C=O); ¹H-NMR (DMSO-d₆/500 MHz): δ 0.98 (3H, d, J=5.4, 6-CH₃-sp.), 1.15-1.23 (2H, m, CH/CH₂-sp.), 1.33-1.42 (1H, m, CH/CH₂-sp.), 1.56 (1H, d, J=6.3, CH/CH₂-sp.), 1.64 (1H, d, J=6.3, CH/CH₂-sp.), 1.72 (1H, d, J=13.6, CH/CH₂-sp.), 1.93-2.01 (3H, m, CH/CH₂-sp.), 2.49-2.50 (5H, m, 3-CH₃-ind., DMSO-d₆), 3.57 (2H, s, C2-H₂-sp.), 7.24 (1H, dd, J=8.5, 1.9, H6-ind.), 7.44 (1H, d, J=8.3, H7-ind.), 7.70 (1H, d, J=1.9, H4-ind.), 10.05, 10.08 (1H, 2s, CONH), 11.50, 11.52 (1H, 2s, NH); ¹³C-NMR (APT) (DMSO-d₆/125 MHz): δ 10.40, 10.46 (3-CH₃-ind.), 16.90 (6-CH₃-sp.), 23.50, 25.39, 29.35, 32.08, 39.15 (CH₂-sp.), 39.32 (C6-sp.), 77.08 (C5-sp.), 114.41, 114.50 (C7-ind.), 115.79 (C3-ind.), 119.93, 119.97 (C4-ind.), 124.68 (C5-ind.), 124.99, 125.10 (C6-ind.), 127.86 (C2-ind.), 129.52 (C3a-ind.), 134.89 (C7a-ind.), 162.51, 163.58 (CO-NH), 168.48, 169.41 (CO-sp.). MS (ESI+) m/z (%): 391.9 ([M+H]⁺, 100), 394.0 ([M+H+2]⁺, 32.2). Anal. Calcd for C₁₉H₂₂ClN₃O₂S (391.91): C, 58.23; H, 5.66; N, 10.72. Found: C, 58.70; H, 5.48; N, 10.66.

4.1.9. 5-Chloro-3-methyl-N-(7-methyl-3-oxo-1-thia-4-azaspiro[4.5]decan-4-yl)-1H-indole-2-carboxamide (4d)

White crystals (45.0%); mp 285-286 °C; IR(KBr): ν_{\max} 3340 (N-H), 1701, 1670 (C=O); ¹H-NMR (DMSO-d₆/500 MHz): δ 0.76-0.82 (1H, m, CH/CH₂-sp.), 0.91 (3H, d*, J=4.8, 7-CH₃-sp.), 1.40-1.88 (8H, m, CH/CH₂-sp.), 2.48-2.52 (5H, m, 3-CH₃-ind., DMSO-d₆), 3.64 (2H, s, C2-H₂-sp.), 7.20 (1H, dd, J=8.7, 1.9, H6-ind.), 7.43 (1H, d, J=8.3, H7-ind.), 7.70 (1H, d, J=1.9, H4-ind.), 10.10 (1H, s, CONH), 11.40 (1H, s, NH); ¹³C-NMR (APT) (DMSO-d₆/125 MHz): δ 10.38, 10.45 (3-CH₃-ind.), 22.75 (7-CH₃-sp.), 23.15, 28.70 (CH₂-sp.), 30.29 (C7-sp.), 33.47, 37.19, 46.00 (CH₂-sp.), 72.90 (C5-sp.), 114.42, 114.51 (C7-ind.), 115.64 (C3-ind.), 119.92, 119.97 (C4-ind.), 124.68 (C5-ind.), 124.99, 125.11 (C6-ind.), 127.81 (C2-ind.), 129.53 (C3a-ind.), 134.92 (C7a-ind.), 162.24 (CO-NH), 168.34 (CO-sp.). Anal. Calcd for C₁₉H₂₂ClN₃O₂S (391.91): C, 58.23; H, 5.66; N, 10.72. Found: C, 57.96; H, 5.75; N, 10.75.

4.1.10. 5-Chloro-3-methyl-N-(8-methyl-3-oxo-1-thia-4-azaspiro[4.5]decan-4-yl)-1H-indole-2-carboxamide (4e)

White needles (54.1%); mp 264-266 °C; IR(KBr): ν_{\max} 3248, 3161 (N-H), 1701, 1654 (C=O); ¹H-NMR (DMSO-d₆/500 MHz): δ 0.87, 0.92 (3H, 2d, J=6.3, 8-CH₃-sp.), 1.10-1.40 (3H, m, CH/CH₂-sp.), 1.52-1.93 (6H, m, CH/CH₂-sp.), 2.44-2.50 (5H, m, 3-CH₃-ind., DMSO-d₆), 3.64, 3.65 (2H, 2s, C2-H₂-sp.), 7.23 (1H, dd, J=8.7, 1.9, H6-ind.), 7.43 (1H, d, J=8.7, H7-ind.), 7.70 (1H, d, J=1.9, H4-ind.), 10.13, 10.21 (1H, 2s, CONH), 11.51, 11.57 (1H, 2s, NH); ¹³C-NMR (APT) (DMSO-d₆/125 MHz): δ 10.43 (3-CH₃-ind.),

32.08, 37.55 (CH₂-sp.), 72.13, 72.95 (C5-sp.), 114.45 (C7-ind.), 115.05, 115.46 (C3-ind.), 119.97 (C4-ind.), 124.65 (C5-ind.), 125.01 (C6-ind.), 127.88 (C2-ind.), 129.52 (C3a-ind.), 134.91, 134.96 (C7a-ind.), 162.25, 162.41 (CONH), 168.39, 168.43 (CO-sp.). MS (ESI-) m/z (%): 390.2 ([M-H]⁻, 100), 392.2 ([M-H+2]⁻, 37.9). Anal. Calcd for C₁₉H₂₂ClN₃O₂S (391.91): C, 58.23; H, 5.66; N, 10.72. Found: C, 58.24; H, 5.35; N, 10.78.

4.1.11. 5-Chloro-N-(8-ethyl-3-oxo-1-thia-4-azaspiro[4.5]decan-4-yl)-3-methyl-1H-indole-2-carboxamide (4f)

White needles (40.2%); mp 264-265 °C; IR(KBr): ν_{\max} 3323 (N-H), 1701, 1685 (C=O); ¹H-NMR (DMSO-d₆/500 MHz): δ 0.84 (3H, t, J=7.3, 8-CH₂CH₃-sp.), 1.02-1.26 (5H, m, CH/CH₂-sp., 8-CH₂CH₃-sp.), 1.60-1.96 (6H, m, CH/CH₂-sp.), 2.48-2.52 (5H, m, 3-CH₃-ind., DMSO-d₆), 3.64, 3.65 (2H, 2s, C2-H₂-sp.), 7.23 (1H, dd, J=8.8, 2.4, H6-ind.), 7.40 (1H, d, J=8.3, H7-ind.), 7.70 (1H, d, J=1.9, H4-ind.), 10.14, 10.18 (1H, 2s, CONH), 11.50, 11.56 (1H, 2s, NH); ¹³C-NMR (APT) (DMSO-d₆/125 MHz): δ 10.39, 10.46 (3-CH₃-ind.), 12.05 (8-CH₂CH₃-sp.), 28.62, 28.71, 29.44, 29.67, 37.53 (CH₂-sp., 8-CH₂CH₃-sp.), 37.89 (C8-sp.), 73.03 (C5-sp.), 114.40, 114.49 (C7-ind.), 115.47 (C3-ind.), 119.94, 119.98 (C4-ind.), 124.66 (C5-ind.), 124.94, 125.06 (C6-ind.), 127.90 (C2-ind.), 129.54 (C3a-ind.), 134.92 (C7a-ind.), 162.24 (CONH), 168.40 (CO-sp.). Anal. Calcd for C₂₀H₂₄ClN₃O₂S (405.94): C, 59.17; H, 5.96; N, 10.35. Found: C, 59.23; H, 6.09; N, 10.49.

4.1.12. 5-Chloro-3-methyl-N-(8-propyl-3-oxo-1-thia-4-azaspiro[4.5]decan-4-yl)-1H-indole-2-carboxamide (4g)

White powder (41.3%); mp 246-247 °C; IR(KBr): ν_{\max} 3316 (N-H), 1701, 1645 (C=O); ¹H-NMR (DMSO-d₆/500 MHz): δ 0.84 (3H, t, J=7.3, 8-CH₂CH₂CH₃-sp.), 1.14-1.31 (7H, m, CH/CH₂-sp., 8-CH₂CH₂CH₃-sp.), 1.74-1.89 (6H, m, CH/CH₂-sp.), 2.48-2.51 (5H, m, 3-CH₃-ind., DMSO-d₆), 3.63 (2H, s, C2-H₂-sp.), 7.23 (1H, dd, J=8.7, 1.9, H6-ind.), 7.43 (1H, d, J=8.8, H7-ind.), 7.70 (1H, d, J=2.0, H4-ind.), 10.11 (1H, s, CONH), 11.48 (1H, s, NH); ¹³C-NMR (APT) (DMSO-d₆/125 MHz): δ 10.39, 10.46 (3-CH₃-ind.), 14.85 (8-CH₂CH₂CH₃-sp.), 20.18 (8-CH₂CH₂CH₃-sp.), 28.63, 29.74, 30.06 (CH₂-sp., 8-CH₂CH₂CH₃-sp.), 35.83 (C8-sp.), 37.51, 39.07 (CH₂-sp.), 73.04 (C5-sp.), 114.40, 114.50 (C7-ind.), 115.54 (C3-ind.), 119.93, 119.97 (C4-ind.), 124.67 (C5-ind.), 124.94, 125.07 (C6-ind.), 127.87 (C2-ind.), 129.54 (C3a-ind.), 134.91 (C7a-ind.), 162.42 (CONH), 168.40 (CO-sp.). MS (ESI+) m/z (%): 420.0 ([M+H]⁺, 100), 421.9 ([M+H+2]⁺, 36.9). Anal. Calcd for C₂₁H₂₆ClN₃O₂S (419.97) C, 60.06; H, 6.24; N, 10.01. Found: C, 59.81; H, 6.02; N, 10.14.

4.1.13. N-(8-tert-butyl-3-oxo-1-thia-4-azaspiro[4.5]decan-4-yl)-5-chloro-3-methyl-1H-indole-2-carboxamide (4h)

Beige crystals (48.1%); mp 252-254 °C; IR(KBr): ν_{\max} 3327, 3179 (N-H), 1692, 1670 (C=O); ¹H-NMR (DMSO-d₆/500 MHz): δ 0.84 (9H, s, 8-C(CH₃)₃-sp.), 0.95-0.98 (1H, m, CH/CH₂-sp.), 1.23-1.28 (2H, m, CH/CH₂-sp.), 1.78 (2H, d, J=12.6, CH/CH₂-sp.), 1.92 (4H, s*, CH/CH₂-sp.), 2.49-2.51 (5H, m, 3-CH₃-ind., DMSO-d₆), 3.63 (2H, s, C2-H₂-sp.), 7.24 (1H, dd, J=8.6, 2.0, H6-ind.), 7.43 (1H, d, J=8.8, H7-ind.), 7.70 (1H, d, J=2.0, H4-ind.), 10.12 (1H, s, CONH), 11.47 (1H, s, NH); ¹³C-NMR (APT) (DMSO-d₆/125 MHz): δ 10.41, 10.48 (3-CH₃-ind.), 24.45 (CH₂-sp.), 28.02 (8-C(CH₃)₃-sp.), 28.61 (CH₂-sp.), 32.66 (8-C(CH₃)₃-sp.), 37.82 (CH₂-sp.), 46.48 (C8-sp.), 72.92 (C5-sp.), 114.40, 114.50 (C7-ind.), 115.55 (C3-ind.), 119.92, 119.97 (C4-ind.), 124.67 (C5-ind.), 124.95, 125.07 (C6-ind.), 127.85 (C2-ind.), 129.54 (C3a-ind.), 134.91 (C7a-ind.), 162.21 (CONH), 168.41 (CO-sp.). Anal. Calcd for C₂₂H₂₈ClN₃O₂S (433.99) C, 60.88; H, 6.50; N, 9.68. Found: C, 60.99; H, 6.42; N, 9.67.

azaspiro[4.5]decan-4-yl)-1H-indole-2-carboxamide (4i)

White powder (42.9%); mp 288-290 °C; IR(KBr): ν_{\max} 3321 (N-H), 1701, 1668 (C=O); ¹H-NMR (DMSO-d₆/500 MHz): δ 0.77 (1H, t, J=12.7, CH/CH₂-sp.), 0.92 (6H, s*, 7-(CH₃)₂-sp.), 1.09 (3H, s*, 9-CH₃-sp.), 1.23-1.37 (2H, m, CH/CH₂-sp.), 1.74-1.89 (4H, m, CH/CH₂-sp.), 2.48-2.51 (5H, m, 3-CH₃-ind., DMSO-d₆), 3.55 (1H, d, J=16.1, C2-H₂-sp.), 3.68 (1H, d, J=15.7, C2-H₂-sp.), 7.24 (1H, dd, J=8.4, 2.0, H6-ind.), 7.44 (1H, d, J=8.3, H7-ind.), 7.69 (1H, d, J=2.0, H4-ind.), 10.06 (1H, s, CONH), 11.49 (1H, s, NH); ¹³C-NMR (APT) (DMSO-d₆/125 MHz): δ 10.35, 10.42 (3-CH₃-ind.), 22.55, 26.30, 27.83 (7-(CH₃)₂, 9-CH₃-sp.), 28.82, 32.53 (CH₂-sp.), 34.57 (C9-sp.), 45.98, 47.52 (CH₂-sp., C7-sp.), 72.21 (C5-sp.), 114.42, 114.51 (C7-ind.), 115.67 (C3-ind.), 119.92, 119.96 (C4-ind.), 124.69 (C5-ind.), 125.00, 125.11 (C6-ind.), 127.84 (C2-ind.), 129.52 (C3a-ind.), 134.92 (C7a-ind.), 162.33 (CONH), 168.33 (CO-sp.). Anal. Calcd for C₂₁H₂₆ClN₃O₂S (419.97): C, 60.06; H, 6.24; N, 10.01. Found: C, 59.73; H, 6.06; N, 10.06.

4.1.15. 5-Chloro-3-methyl-N-(8-phenyl-3-oxo-1-thia-4-azaspiro[4.5]decan-4-yl)-1H-indole-2-carboxamide (4j)

White crystals (61.8%); mp 161-163 °C; IR(KBr): ν_{\max} 3325, 3194 (N-H), 1705, 1653 (C=O); ¹H-NMR (DMSO-d₆/500 MHz): δ 1.06 (1H, t, J=7.0, CH₂-sp.), 1.70 (2H, q, J=12.6, CH₂-sp.), 1.90 (2H, d*, J=12.2, CH₂-sp.), 1.99 (2H, d*, J=11.2, CH₂-sp.), 2.15 (1H, s*, CH₂-sp.), 2.49-2.52 (5H, m, 3-CH₃-ind., DMSO-d₆), 2.54 (1H, s, CH-sp.), 3.69 (2H, s, C2-H₂-sp.), 7.19 (1H, tt, J=7.3, 1.5, 8-C₆H₅(H4)-sp.), 7.23 (2H, dd, J=7.5, 1.5, 8-C₆H₅(H2,H6)-sp.), 7.25 (1H, dd, J=8.8, 2.0, H6-ind.), 7.29 (2H, t, J=7.3, 8-C₆H₅(H3,H5)-sp.), 7.46 (1H, d, J=8.8, H7-ind.), 7.72 (1H, d, J=2.4, H4-ind.), 10.18 (1H, s, CONH), 11.51 (1H, s, NH); ¹³C-NMR (APT) (DMSO-d₆/125 MHz): δ 10.46, 10.53 (3-CH₃-ind.), 28.69, 31.21, 37.77 (CH₂-sp.), 42.24 (C8-sp.), 56.74 (CH₂-sp.), 72.47 (C5-sp.), 114.42, 114.52 (C7-ind.), 115.65 (C3-ind.), 119.97, 120.00 (C4-ind.), 124.70 (C5-ind.), 125.00, 125.12 (C6-ind.), 127.21, 127.34 (8-ar.(CH)-sp.), 127.85 (C2-ind.), 129.01, 129.14 (8-ar.(CH)-sp.), 129.57 (C3a-ind.), 134.94 (C7a-ind.), 146.55 (8-ar.(C)-sp.), 162.29 (CONH), 168.46 (CO-sp.). MS (ESI+) m/z (%): 453.9 ([M+H]⁺, 100), 455.9 ([M+H+2]⁺, 36.6). Anal. Calcd for C₂₄H₂₄ClN₃O₂S (453.98) C, 63.49; H, 5.33; N, 9.26. Found: C, 63.41; H, 5.22; N, 9.06.

4.1.16. 5-Chloro-3-methyl-N-(2-methyl-3-oxo-1-thia-4-azaspiro[4.4]nonan-4-yl)-1H-indole-2-carboxamide (5a)

White powder (60.2%); mp 282-284 °C; IR(KBr): ν_{\max} 3307 (N-H), 1694, 1651 (C=O); ¹H-NMR (DMSO-d₆/500 MHz): δ 1.47 (3H, d, J=7.3, 2-CH₃-sp.), 1.64-1.72 (4H, m, CH₂-sp.), 1.83-1.95 (2H, m, CH₂-sp.), 2.18-2.30 (2H, m, CH₂-sp.), 2.49-2.51 (6H, m, 3-CH₃-ind., DMSO-d₆), 3.99 (1H, q, J=6.8, C2-H-sp.), 7.24 (1H, dd, J=8.8, 2.0, H6-ind.), 7.43 (1H, d, J=9.2, H7-ind.), 7.70 (1H, d, J=2.0, H4-ind.), 10.20 (1H, s, CONH), 11.50 (1H, s, NH); ¹³C-NMR (APT) (DMSO-d₆/125 MHz): δ 10.35, 10.43 (3-CH₃-ind.), 20.09 (2-CH₃-sp.), 23.47, 23.51 (CH₂-sp.), 38.35, 38.49 (C2-sp.), 39.32 (CH₂-sp.), 75.01 (C5-sp.), 114.43, 114.53 (C7-ind.), 115.37 (C3-ind.), 119.96, 120.00 (C4-ind.), 124.69 (C5-ind.), 125.00, 125.12 (C6-ind.), 127.82 (C2-ind.), 129.53 (C3a-ind.), 134.97 (C7a-ind.), 162.27 (CO-NH), 171.07 (CO-sp.). MS (ESI-) m/z (%): 376.3 ([M-H]⁻, 100), 378.2 ([M-H+2]⁻, 37.2). Anal. Calcd for C₁₈H₂₀ClN₃O₂S (377.89): C, 57.21; H, 5.33; N, 11.12. Found: C, 57.37; H, 5.24; N, 11.19.

4.1.17. 5-Chloro-3-methyl-N-(2-methyl-3-oxo-1-thia-4-azaspiro[4.5]decan-4-yl)-1H-indole-2-carboxamide (5b)

White needles (40.1%); mp 281-283 °C; IR(KBr): ν_{\max} 3311 (N-H), 1693, 1654 (C=O); ¹H-NMR (DMSO-d₆/500 MHz): δ 1.03-1.09

(1H, 2-CH₃-sp.), 1.70-2.00 (6H, m, CH₂-sp.), 2.48-2.50 (5H, m, 3-CH₃-ind., DMSO-d₆), 3.95 (1H, q, J=7.3, C2-H-sp.), 7.24 (1H, dd, J=8.7, 1.9, H6-ind.), 7.43 (1H, d, J=8.8, H7-ind.), 7.70 (1H, d, J=1.9, H4-ind.), 10.10 (1H, s, CONH), 11.50 (1H, s, NH); ¹³C-NMR (HSQC) (DMSO-d₆/125 MHz): δ 10.43 (3-CH₃-ind.), 20.77 (2-CH₃-sp.), 23.46, 23.88, 24.74 (CH₂-sp.), 37.49, 37.92 (CH₂-sp., C2-sp.), 38.83 (CH₂-sp.), 71.53 (C5-sp.), 114.45 (C7-ind.), 115.46 (C3-ind.), 119.97 (C4-ind.), 124.65 (C5-ind.), 125.01 (C6-ind.), 127.88 (C2-ind.), 129.50 (C3a-ind.), 134.90 (C7a-ind.), 162.23 (CO-NH), 170.99 (CO-sp.). Anal. Calcd for C₁₉H₂₂ClN₃O₂S (391.91): C, 58.23; H, 5.66; N, 10.72. Found: C, 57.78; H, 5.47; N, 10.64.

4.1.18. N-(2,6-dimethyl-3-oxo-1-thia-4-azaspiro[4.5]decan-4-yl)-5-chloro-3-methyl-1H-indole-2-carboxamide (5c)

White flakes (55.7%); mp 261-264 °C; IR(KBr): ν_{max} 3217, 3134 (N-H), 1701, 1645 (C=O); ¹H-NMR (DMSO-d₆/500 MHz): δ 0.98 (3H, d*, J=5.9, 6-CH₃-sp.), 1.14-1.35 (3H, m, CH/CH₂-sp.), 1.44, 1.45 (3H, 2d, J=6.8, 7.3, 2-CH₃-sp.), 1.54-1.58 (1H, m, CH/CH₂-sp.), 1.63 (1H, d*, J=8.3, CH/CH₂-sp.), 1.72 (1H, d*, J=13.6, CH/CH₂-sp.), 1.88-2.00 (3H, m, CH/CH₂-sp.), 2.49-2.51 (5H, m, 3-CH₃-ind., DMSO-d₆), 3.84, 3.94 (1H, 2q, J=6.8, C2-H-sp.), 7.24 (1H, dd, J=8.5, 2.0, H6-ind.), 7.43, 7.44 (1H, 2d, J=8.3, H7-ind.), 7.70 (1H, d, J=2.0, H4-ind.), 10.08 (1H, s*, CONH), 11.51 (1H, s, NH); ¹³C-NMR (APT) (DMSO-d₆/125 MHz): δ 10.39, 10.46 (3-CH₃-ind.), 16.95 (6-CH₃-sp.), 23.46, 25.41, 29.71, 32.24 (CH₂-sp.), 38.11, 38.31 (C2-sp.), 39.26 (C6-sp.), 75.58, 75.98 (C5-sp.), 114.40, 114.48 (C7-ind.), 115.71 (C3-ind.), 119.94, 119.97 (C4-ind.), 124.67 (C5-ind.), 124.97, 125.09 (C6-ind.), 127.89 (C2-ind.), 129.53 (C3a-ind.), 134.88 (C7a-ind.), 162.48 (CO-NH), 170.97, 171.09 (CO-sp.). Anal. Calcd for C₂₀H₂₄ClN₃O₂S (405.94): C, 59.17; H, 5.96; N, 10.35. Found: C, 59.21; H, 5.68; N, 10.11.

4.1.19. N-(2,7-dimethyl-3-oxo-1-thia-4-azaspiro[4.5]decan-4-yl)-5-chloro-3-methyl-1H-indole-2-carboxamide (5d)

White crystals (46.0%); mp 214-216 °C; IR(KBr): ν_{max} 3408, 3304 (O-H/N-H), 1697, 1654 (C=O); ¹H-NMR (DMSO-d₆/500 MHz): δ 0.75-0.83 (1H, m, CH/CH₂-sp.), 0.91 (3H, d, J=5.8, 7-CH₃-sp.), 1.06 (3H, t, J=7.3, CH₂CH₂OH), 1.48 (3H, d, J=7.3, 2-CH₃-sp.), 1.50-2.00 (8H, m, CH/CH₂-sp.), 2.48-2.52 (5H, m, 3-CH₃-ind., DMSO-d₆), 3.43 (2H, m, CH₃CH₂OH), 3.92-3.97 (1H, m, C2-H-sp.), 4.34 (1H, t, J=6.8, CH₃CH₂OH), 7.25 (1H, dd, J=8.7, 1.9, H6-ind.), 7.44 (1H, d, J=8.7, H7-ind.), 7.72 (1H, d, J=1.9, H4-ind.), 10.50 (1H, s, CONH), 11.50 (1H, s, NH); ¹³C-NMR (HSQC) (DMSO-d₆/125 MHz): δ 10.44 (3-CH₃-ind.), 19.27 (CH₃CH₂OH), 20.65 (2-CH₃-sp.), 22.70 (7-CH₃-sp.), 23.42 (CH₂-sp.), 30.17 (C7-sp.), 30.60, 33.47 (CH₂-sp.), 38.30 (C2-sp.), 38.83, 46.00 (CH₂-sp.), 56.74 (CH₃CH₂OH), 71.54 (C5-sp.), 114.47 (C7-ind.), 115.59 (C3-ind.), 119.98 (C4-ind.), 124.66 (C5-ind.), 125.04 (C6-ind.), 127.84 (C2-ind.), 129.54 (C3a-ind.), 134.90 (C7a-ind.), 162.22 (CO-NH), 170.91 (CO-sp.). MS (ESI-) m/z (%): 404.1 ([M-H]⁻, 100), 406.1 ([M-H+2]⁻, 28.4). Anal. Calcd for C₂₀H₂₄ClN₃O₂S·CH₃CH₂OH (405.94+46.07): C, 58.41; H, 6.63; N, 9.29. Found: C, 58.20; H, 6.54; N, 9.26.

4.1.20. N-(2,8-dimethyl-3-oxo-1-thia-4-azaspiro[4.5]decan-4-yl)-5-chloro-3-methyl-1H-indole-2-carboxamide (5e)

White crystals (75.3%); mp 235-238 °C; IR(KBr): ν_{max} 3321, 3246 (N-H), 1701, 1678 (C=O); ¹H-NMR (DMSO-d₆/500 MHz): δ 0.88, 0.94 (3H, 2d, J=6.8, 8-CH₃-sp.), 1.12-1.38 (4H, m, CH/CH₂-sp.), 1.48 (3H, d, J=7.3, 2-CH₃-sp.), 1.60-2.10 (5H, m, CH/CH₂-sp.), 2.48-2.52 (5H, m, 3-CH₃-ind., DMSO-d₆), 3.96 (1H, q, J=7.3, C2-H-sp.), 7.24 (1H, dd, J=8.7, 1.9, H6-ind.), 7.44 (1H, d, J=8.7, H7-ind.), 7.70 (1H, d, J=1.9, H4-ind.), 10.18, 10.26 (1H, 2s, CONH), 11.52, 11.58 (1H, 2s, NH); ¹³C-NMR (HMBC) (DMSO-d₆/125 MHz): δ 10.43 (CH₃-ind.), 20.56 (2-CH₃-sp.), 22.54 (8-CH₃-

sp.), 71.39 (C5-sp.), 114.95 (C7-ind.), 115.45 (C3-ind.), 119.97 (C4-ind.), 124.66 (C6-ind.), 125.01 (C5-ind.), 127.90 (C2-ind.), 129.54 (C3a-ind.), 134.91 (C7a-ind.), 162.23 (CONH), 171.06 (C=O). Anal. Calcd for C₂₀H₂₄ClN₃O₂S (405.94): C, 59.17; H, 5.96; N, 10.35. Found: C, 59.06; H, 6.21; N, 10.32.

4.1.21. 5-Chloro-N-(8-ethyl-2-methyl-3-oxo-1-thia-4-azaspiro[4.5]decan-4-yl)-3-methyl-1H-indole-2-carboxamide (5f)

White crystals (52.1%); mp 258-261 °C; IR(KBr): ν_{max} 3317, 3265 (N-H), 1701, 1653 (C=O); ¹H-NMR (DMSO-d₆/500 MHz): δ 0.85 (3H, t, J=7.3, 8-CH₂CH₃-sp.), 1.00-1.30 (5H, m, CH/CH₂-sp., 8-CH₂CH₃-sp.), 1.45 (3H, d, J=6.8, 2-CH₃-sp.), 1.70-1.90 (6H, m, CH/CH₂-sp.), 2.48-2.52 (5H, m, 3-CH₃-ind., DMSO-d₆), 3.93 (1H, q, J=6.8, C2-H-sp.), 7.32 (1H, dd, J=8.7, 1.9, H6-ind.), 7.43 (1H, d, J=8.6, H7-ind.), 7.70 (1H, d, J=1.9, H4-ind.), 10.18, 10.22 (1H, 2s, CONH), 11.50, 11.56 (1H, 2s, NH); ¹³C-NMR (APT) (DMSO-d₆/125 MHz): δ 10.39, 10.45 (CH₃-ind.), 12.03 (8-CH₂CH₃-sp.), 20.65 (2-CH₃-sp.), 28.45, 29.50, 29.95 (CH₂-sp., 8-CH₂CH₃-sp.), 37.45, 37.60, 37.85 (C2-sp., C8-sp.), 71.68 (C5-sp.), 114.40, 114.49 (C7-ind.), 115.43 (C3-ind.), 119.94, 119.98 (C4-ind.), 124.66 (C6-ind.), 124.94, 125.05 (C5-ind.), 127.92 (C2-ind.), 129.55 (C3a-ind.), 134.92 (C7a-ind.), 162.22 (CONH), 171.04 (C=O). MS (ESI-) m/z (%): 418.2 ([M-H]⁻, 100), 420.2 ([M-H+2]⁻, 37.4). Anal. Calcd for C₂₁H₂₆ClN₃O₂S (419.97): C, 60.06; H, 6.24; N, 10.01. Found: C, 60.12; H, 6.18; N, 9.96.

4.1.22. 5-Chloro-3-methyl-N-(2-methyl-8-propyl-3-oxo-1-thia-4-azaspiro[4.5]decan-4-yl)-1H-indole-2-carboxamide (5g)

White crystals (42.3%); mp 173-176 °C; IR(KBr): ν_{max} 3329, 3254 (N-H), 1709, 1648 (C=O); ¹H-NMR (DMSO-d₆/500 MHz): δ 0.84 (3H, t, J=7.3, 8-CH₂CH₂CH₃-sp.), 1.14-1.31 (7H, m, CH/CH₂-sp., 8-CH₂CH₂CH₃-sp.), 1.46 (3H, d, J=7.3, 2-CH₃-sp.), 1.75-1.91 (6H, m, CH/CH₂-sp.), 2.49-2.52 (5H, m, 3-CH₃-ind., DMSO-d₆), 3.92 (1H, q, J=6.8, C2-H-sp.), 7.23 (1H, dd, J=8.8, 2.0, H6-ind.), 7.42, 7.43 (1H, 2d, J=8.8, H7-ind.), 7.70 (1H, d, J=2.0, H4-ind.), 10.16, 10.23 (1H, 2s, CONH), 11.48, 11.57 (1H, 2s, NH); ¹³C-NMR (APT) (DMSO-d₆/125 MHz): δ 10.39, 10.46 (3-CH₃-ind.), 14.85 (8-CH₂CH₂CH₃-sp.), 20.19 (8-CH₂CH₂CH₃-sp.), 20.63 (2-CH₃-sp.), 29.86, 29.92, 30.34 (CH₂-sp., 8-CH₂CH₂CH₃-sp.), 35.81 (C8-sp.), 37.44, 37.59 (C2-sp.), 39.09 (CH₂-sp., 8-CH₂CH₂CH₃-sp.), 71.58, 71.68 (C5-sp.), 114.38, 114.49 (C7-ind.), 115.50 (C3-ind.), 119.92, 119.97 (C4-ind.), 124.67 (C5-ind.), 124.94, 125.06 (C6-ind.), 127.88 (C2-ind.), 129.55 (C3a-ind.), 134.91, 134.98 (C7a-ind.), 162.20, 162.45 (CONH), 171.04 (CO-sp.). Anal. Calcd for C₂₂H₂₈ClN₃O₂S (433.99): C, 60.88; H, 6.50; N, 9.68. Found: C, 60.58; H, 6.33; N, 9.61.

4.1.23. N-(2-methyl-8-tert-butyl-3-oxo-1-thia-4-azaspiro[4.5]decan-4-yl)-5-chloro-3-methyl-1H-indole-2-carboxamide (5h)

White powder (53.5%); mp 226-228 °C; IR(KBr): ν_{max} 3308 (N-H), 1698, 1658 (C=O); ¹H-NMR (DMSO-d₆/500 MHz): δ 0.84 (9H, s, 8-C(CH₃)₃-sp.), 0.96 (1H, t*, J=12.2, CH/CH₂-sp.), 1.17-1.32 (2H, m, CH/CH₂-sp.), 1.46 (3H, d, J=6.8, 2-CH₃-sp.), 1.78 (2H, d, J=12.2, CH/CH₂-sp.), 1.89-1.95 (4H, m, CH/CH₂-sp.), 2.49-2.53 (5H, m, 3-CH₃-ind., DMSO-d₆), 3.93 (1H, q, J=6.8, C2-H-sp.), 7.23 (1H, dd, J=8.8, 2.0, H6-ind.), 7.43 (1H, d, J=8.8, H7-ind.), 7.70 (1H, d, J=2.0, H4-ind.), 10.16 (1H, s, CONH), 11.47 (1H, s, NH); ¹³C-NMR (APT) (DMSO-d₆/125 MHz): δ 10.40, 10.46 (3-CH₃-ind.), 20.04 (2-CH₃-sp.), 24.30, 24.71 (CH₂-sp.), 28.01 (8-C(CH₃)₃-sp.), 32.67 (8-C(CH₃)₃-sp.), 37.45, 37.60 (C2-sp.), 46.42 (C8-sp.), 71.58 (C5-sp.), 114.39, 114.49 (C7-ind.), 115.50 (C3-ind.), 119.93, 119.97 (C4-ind.), 124.66 (C5-ind.), 124.96, 125.05 (C6-ind.), 127.87 (C2-ind.), 129.55 (C3a-ind.), 134.91 (C7a-ind.), 162.19 (CONH), 171.06 (CO-sp.). MS (ESI-) m/z (%): 446.4 ([M-H]⁻,

(448.02) C, 61.66; H, 6.75; N, 9.38. Found: C, 61.88; H, 6.84; N, 9.44.

4.1.24. 5-Chloro-3-methyl-N-(2,7,7,9-tetramethyl-3-oxo-1-thia-4-azaspiro[4.5]decan-4-yl)-1H-indole-2-carboxamide (5i)

White flakes (47.7%); mp 263-265 °C; IR(KBr): ν_{\max} 3312 (N-H), 1699, 1660 (C=O); ¹H-NMR (DMSO-*d*₆/500 MHz): δ 0.77 (1H, t*, J=12.8, CH/CH₂-sp.), 0.92 (6H, s, 7-(CH₃)₂-sp.), 1.09 (3H, d, J=10.7, 9-CH₃-sp.), 1.23-1.37 (2H, m, CH/CH₂-sp.), 1.46, 1.47 (3H, 2d, J=7.3, 2-CH₃-sp.), 1.70-1.89 (4H, m, CH/CH₂-sp.), 2.49-2.51 (5H, m, 3-CH₃-ind., DMSO-*d*₆), 3.89, 3.94 (1H, 2q, J=6.8, C2-H-sp.), 7.24 (1H, dd, J=8.7, 2.0, H6-ind.), 7.44 (1H, d, J=8.8, H7-ind.), 7.70 (1H, d, J=2.0, H4-ind.), 10.10, 10.11 (1H, 2s, CONH), 11.48, 11.50 (1H, 2s, NH); ¹³C-NMR (APT) (DMSO-*d*₆/125 MHz): δ 10.35, 10.40 (3-CH₃-ind.), 18.89 (2-CH₃-sp.), 22.51, 22.68, 25.98, 26.53, 27.80, 27.90 (7,7,9-CH₃-sp.), 29.88, 32.56 (CH₂-sp.), 34.54, 34.65 (C9-sp.), 37.12, 37.26 (C2-sp.), 45.93, 47.50 (CH₂-sp., C7-sp.), 70.73 (C5-sp.), 114.42, 114.50 (C7-ind.), 115.65 (C3-ind.), 119.92, 119.96 (C4-ind.), 124.67 (C5-ind.), 124.98, 125.10 (C6-ind.), 127.84 (C2-ind.), 129.52 (C3a-ind.), 134.92 (C7a-ind.), 162.34 (CONH), 170.91 (CO-sp.). MS (ESI+) m/z (%): 434.0 ([M+H]⁺, 100), 435.9 ([M+H]+2]⁺, 34.7). Anal. Calcd for C₂₂H₂₈ClN₃O₂S (433.99): C, 60.88; H, 6.50; N, 9.68. Found: C, 60.63; H, 6.36; N, 9.58.

4.1.25. 5-Chloro-3-methyl-N-(2-methyl-8-phenyl-3-oxo-1-thia-4-azaspiro[4.5]decan-4-yl)-1H-indole-2-carboxamide (5j)

White flakes (67.9%); mp 162-164 °C; IR(KBr): ν_{\max} 3323, 3188 (N-H), 1693, 1653 (C=O); ¹H-NMR (DMSO-*d*₆/500 MHz): δ 1.06 (2H, t, J=7.0, CH₂-sp.), 1.49 (3H, d, J=6.8, 2-CH₃-sp.), 1.63-2.25 (6H, m, CH₂-sp.), 2.49-2.51 (5H, m, 3-CH₃-ind., DMSO-*d*₆), 2.55 (1H, s, CH-sp.), 3.99 (1H, q, J=6.8, C2-H-sp.), 7.18 (1H, tt, J=7.5, 1.5, 8-C₆H₅(H4)-sp.), 7.22 (2H, dd, J=7.4, 1.5, 8-C₆H₅(H2,H6)-sp.), 7.25 (1H, dd, J=8.8, 2.0, H6-ind.), 7.30 (2H, t, J=7.3, 8-C₆H₅(H3,H5)-sp.), 7.46 (1H, d, J=9.2, H7-ind.), 7.72 (1H, d, J=2.0, H4-ind.), 10.23 (1H, s, CONH), 11.52 (1H, s, NH); ¹³C-NMR (APT) (DMSO-*d*₆/125 MHz): δ 10.46, 10.53 (3-CH₃-ind.), 20.58 (2-CH₃-sp.), 31.00, 31.56 (CH₂-sp.), 37.55, 37.69 (C2-sp.), 37.75 (CH₂-sp.), 42.26 (C8-sp.), 56.75 (CH₂-sp.), 71.12 (C5-sp.), 114.41, 114.51 (C7-ind.), 115.62 (C3-ind.), 119.97, 120.00 (C4-ind.), 124.71 (C5-ind.), 125.00, 125.12 (C6-ind.), 126.74, 127.05 (8-ar.(CH)-sp.), 127.87 (C2-ind.), 129.01, 129.14 (8-ar.(CH)-sp.), 129.58 (C3a-ind.), 134.95 (C7a-ind.), 146.55 (8-ar.(C)-sp.), 162.28 (CONH), 171.09 (CO-sp.). MS (ESI-) m/z (%): 466.6 ([M-H]⁻, 100), 468.5 ([M-H]+2]⁻, 34.6). Anal. Calcd for C₂₅H₂₆ClN₃O₂S (468.01) C, 64.16; H, 5.60; N, 8.98. Found: C, 64.39; H, 5.75; N, 8.59.

4.2. Biological methods

Inhibitory activity against influenza virus was determined in a CPE reduction assay, described in full detail elsewhere.¹⁸ Briefly, semiconfluent cultures of Madin-Darby canine kidney (MDCK) cells (kindly donated by M. Matrosovich, Marburg, Germany) in 96-well plates were infected with influenza A/H1N1 (strain A/Ned/378/05; a kind gift from R. Fouchier, Rotterdam, the Netherlands); A/H3N2 (A/HK/7/87; from ATCC); or influenza B virus (B/Ned/537/05; also from R. Fouchier) at a multiplicity of infection of 0.0004 plaque-forming units per cell. At the same time, the compounds were added at serial dilutions. After four days incubation at 35 °C, microscopy was performed to score the compounds' inhibitory effect on viral CPE, expressed as 50% effective concentration (EC₅₀), and cytotoxicity, expressed as the minimal cytotoxic concentration (MCC; compound concentration

the colorimetric MTS cell viability assay (CellTiter 96[®] AQueous One Solution Cell Proliferation Assay from Promega) was done, the results of which were expressed as antiviral EC₅₀ and 50% cytotoxic concentration (CC₅₀).³⁵

The polykaryon assay (see¹⁸ for all details) was performed with pCAGEN plasmids expressing wild-type or mutant (E57₂K and D112₂N) forms of H3 HA (cloned from strain A/X-31). HeLa cells seeded into 12-well plates were transfected with HA plasmid using Fugene 6[®] reagent (Promega). Two days later, the HA was activated by brief exposure to TPCK-treated trypsin. After two rinses with PBS containing Ca²⁺ and Mg²⁺ (PBS-CM), the cells were pre-incubated with compound during 15 min. Next, the cells were exposed to acidic buffer (PBS-CM adapted to pH 5) containing compound, and incubated for exactly 15 min at 37 °C. The wells were rinsed with PBS-CM, after which medium with 10% fetal calf serum was added. After 3 h incubation, the cells were fixated with ethanol and stained with Giemsa. Microscopy at 200x magnification was used to count the number of polykaryons (containing five or more nuclei) in four randomly selected microscopic fields.

4.3. Molecular docking studies

Unless stated otherwise, all calculations were done using the Schrödinger Suite (version 2015-4, Schrödinger, LLC, New York, NY, 2015).

For ligand preparation, the selected ligand was drawn with the 2D Sketcher in Maestro and the LigPrep tool (version 2.5) was used to generate the 3D conformers. Tautomers and ionization state of the ligands were determined at neutral pH using Epik.^{36,37} Stereoisomers were generated with one low-energy ring conformation for each stereoisomer.

The cocrystal structures of H3 HA with TBHQ (PDB ID: 3EYM; H3 HA sequence A/Aichi/2/1968) and arbidol (PDB ID: 5T6N; H3 HA sequence A/Hong Kong/1/1968) were retrieved and the proteins were prepared by removing the ligands from the respective hydrophobic pockets and applying the Protein Preparation Wizard.³⁸ Coordinates for the missing residues and missing atoms were filled. In both PDB entries, only the last four residues are missing in the coordinate sets and the residues in the ligand binding site are all resolved. Prior to docking, the protein structures were energy minimized. The Glide grid, defined by taking the centroid of the cocrystallized ligands as the box center, included residues R54₂, L55₂, E57₂ of monomer 1 (chain D in PDB 5T6N) and Y94₂, E97₂ and L99₂ of monomer 2 (chain F in PDB 5T6N).

The ligand was docked into the binding site between monomer 1 (chain C and D in 5T6N) and monomer 2 (chain E and F) according to the Induced Fit Docking (IFD) protocol, which is based on combining Prime energy and GlideScore³⁹⁻⁴¹ and in which side chains in the binding site are allowed to reorient.⁴⁰ The poses were ranked based on Glide Gscore values and the top ranking poses in which the indole group of the spirothiazolidinones is positioned similar to that of the arbidol ligand were selected for visual analysis of the protein – compound interactions.

Acknowledgments

This work was supported in part by the Research Fund of Istanbul University (Project Number T-20867). E.O. would like to thank Prof. Amedeo Caflisch for hosting her during her sabbatical

References and notes

- Uyeki TM. Preventing and controlling influenza with available interventions, *N Engl J Med*. 2014;370:789-791.
- Neumann G, Noda T, Kawaoka Y. Emergence and pandemic potential of swine-origin H1N1 influenza virus, *Nature*. 2009;459:931-939.
- Treanor JJ. Clinical practice. Influenza vaccination, *N Engl J Med*. 2016;375:1261-1268.
- Cobey S, Gouma S, Parkhouse K, Chambers BS, Ertl HC, Schmadler KE, Halpin RA, Lin X, Stockwell TB, Das SR, Landon E, Tesic V, Youngster I, Pinsky BA, Wentworth DE, Hensley SE, Grad YH. Poor immunogenicity, not vaccine strain egg adaptation, may explain the low H3N2 influenza vaccine effectiveness in 2012-13, *Clin Infect Dis*. 2018;67:327-333.
- Kwok KO, Riley S, Perera R, Wei VWI, Wu P, Wei L, Chu DKW, Barr IG, Malik Peiris JS, Cowling BJ. Relative incidence and individual-level severity of seasonal influenza A H3N2 compared with 2009 pandemic H1N1, *BMC Infect Dis*. 2017;17:337.
- Nguyen-Van-Tam JS, Venkatesan S, Muthuri SG, Myles PR. Neuraminidase inhibitors: who, when, where?, *Clin Microbiol Infect*. 2015;21:222-225.
- Moscona A. Global transmission of oseltamivir-resistant influenza, *N Engl J Med*. 2009;360:953-956.
- Naesens L, Stevaert A, Vanderlinden E. Antiviral therapies on the horizon for influenza, *Curr Opin Pharmacol*. 2016;30:106-115.
- Stevaert A, Naesens L. The influenza virus polymerase complex: an update on its structure, functions, and significance for antiviral drug design, *Med Res Rev*. 2016;36:1127-1173.
- Takashita E, Ejima M, Ogawa R, Fujisaki S, Neumann G, Furuta Y, Kawaoka Y, Tashiro M, Odagiri T. Antiviral susceptibility of influenza viruses isolated from patients pre- and post-administration of favipiravir, *Antiviral Res*. 2016;132:170-177.
- Hayden FG, Sugaya N, Hirotsu N, Lee N, de Jong MD, Hurt AC, Ishida T, Sekino H, Yamada K, Portsmouth S, Kawaguchi K, Shishido T, Arai M, Tsuchiya K, Uehara T, Watanabe A, Baloxavir Marboxil Investigators G. Baloxavir marboxil for uncomplicated influenza in adults and adolescents, *N Engl J Med*. 2018;379:913-923.
- Byrd-Leotis L, Cummings RD, Steinhauer DA. The interplay between the host receptor and influenza virus hemagglutinin and neuraminidase, *Int J Mol Sci*. 2017;18:1541.
- Russell CJ. Acid-induced membrane fusion by the hemagglutinin protein and its role in influenza virus biology, *Curr Top Microbiol Immunol*. 2014;385:93-116.
- Edinger TO, Pohl MO, Stertz S. Entry of influenza A virus: host factors and antiviral targets, *J Gen Virol*. 2014;95:263-277.
- Vanderlinden E, Naesens L. Emerging antiviral strategies to interfere with influenza virus entry, *Med Res Rev*. 2014;34:301-339.
- Kadam RU, Wilson IA. Structural basis of influenza virus fusion inhibition by the antiviral drug Arbidol, *Proc Natl Acad Sci U S A*. 2017;114:206-214.
- Russell RJ, Kerry PS, Stevens DJ, Steinhauer DA, Martin SR, Gamblin SJ, Skehel JJ. Structure of influenza hemagglutinin in complex with an inhibitor of membrane fusion, *Proc Natl Acad Sci U S A*. 2008;105:17736-17741.
- Vanderlinden E, Göktas F, Cesur Z, Froeyen M, Reed ML, Russell CJ, Cesur N, Naesens L. Novel inhibitors of influenza virus fusion: structure-activity relationship and interaction with the viral hemagglutinin, *J Virol*. 2010;84:4277-4288.
- Göktaş F, Vanderlinden E, Naesens L, Cesur N, Cesur Z. Microwave assisted synthesis and anti-influenza virus activity of 1-adamantyl substituted N-(1-thia-4-azaspiro[4.5]decan-4-yl)carboxamide derivatives, *Bioorg Med Chem*. 2012;20:7155-7159.
- Göktaş F, Vanderlinden E, Naesens L, Cesur Z, Cesur N, Taş P. Synthesis and structure-activity relationship of N-(3-oxo-1-thia-4-azaspiro[4.5]decan-4-yl)carboxamide inhibitors of influenza virus hemagglutinin mediated fusion, *Phosphorus, Sulfur, and Silicon and the Related Elements*. 2014;190:1075-1087.
- Lanzavecchia A. Tackling influenza with broadly neutralizing antibodies, *Curr Opin Virol*. 2017;24:60-69.
- van Dongen MJP, Kadam RU, Juraszek J, Lawson E, Brandenburg B, Schmitz F, Schepens WBG, Stoops B, van Diepen HA, Jongeneelen M, Tang C, Vermond J, van Eijgen-Obregoso Real A, Blokland S, Garg D, Yu W, Goutier W, Lanckacker E, Klap JM, Peeters DCG, Wu J, Buyck C, Jonckers THM, Roymans D, Roevens P, Vogels R, Koudstaal W, Friesen RHE, Raboisson P, Dhanak D, Goudsmit J, Wilson IA. A small-molecule fusion inhibitor of influenza virus is orally active in mice, *Science*. 2019;363.
- Leneva IA, Falynskova IN, Makhmudova NR, Poromov AA, Yatsyshina SB, Maleev VV. Umifenovir susceptibility monitoring and characterization of influenza viruses isolated during ARBITR clinical study, *J Med Virol*. 2019;91:588-597.
- Blaising J, Polyak SJ, Pecheur EI. Arbidol as a broad-spectrum antiviral: an update, *Antiviral Res*. 2014;107:84-94.
- Leiva R, Barniol-Xicota M, Codony S, Ginex T, Vanderlinden E, Montes M, Caffrey M, Luque FJ, Naesens L, Vazquez S. Aniline-based inhibitors of influenza H1N1 virus acting on hemagglutinin-mediated fusion, *J Med Chem*. 2018;61:98-118.
- Rajur SB, Merwade AY, Basanagoudar LD, Kulkarni PV. Synthesis and antimicrobial activity of new substituted 10-methyl-1,2-dihydro-1-oxo-1,2,4-triazino(4,5-a)indoles, *J Pharm Sci*. 1989;78:780-782.
- Cihan-Ustundag G, Capan G. Synthesis and evaluation of functionalized indoles as antimycobacterial and anticancer agents, *Molecular diversity*. 2012;16:525-539.
- Thoennes S, Li ZN, Lee BJ, Langley WA, Skehel JJ, Russell RJ, Steinhauer DA. Analysis of residues near the fusion peptide in the influenza hemagglutinin structure for roles in triggering membrane fusion, *Virology*. 2008;370:403-414.
- Daniels RS, Downie JC, Hay AJ, Knossow M, Skehel JJ, Wang ML, Wiley DC. Fusion mutants of the influenza virus hemagglutinin glycoprotein, *Cell*. 1985;40:431-439.
- Hoffman LR, Kuntz ID, White JM. Structure-based identification of an inducer of the low-pH conformational change in the influenza virus hemagglutinin: irreversible inhibition of infectivity, *J Virol*. 1997;71:8808-8820.
- Han J, Burgess K. Fluorescent indicators for intracellular pH, *Chem Rev*. 2010;110:2709-2728.
- Snyder PW, Mecinovic J, Moustakas DT, Thomas SW, 3rd, Harder M, Mack ET, Lockett MR, Heroux A, Sherman W, Whitesides GM. Mechanism of the hydrophobic effect in the biomolecular recognition of arylsulfonamides by carbonic anhydrase, *Proc Natl Acad Sci U S A*. 2011;108:17889-17894.
- Kadam RU, Wilson IA. A small-molecule fragment that emulates binding of receptor and broadly neutralizing antibodies to influenza A hemagglutinin, *Proc Natl Acad Sci U S A*. 2018;115:4240-4245.
- Leneva IA, Russell RJ, Boriskin YS, Hay AJ. Characteristics of arbidol-resistant mutants of influenza virus: implications for the mechanism of anti-influenza action of arbidol, *Antiviral Res*. 2009;81:132-140.
- Vrijens P, Noppen S, Boogaerts T, Vanstreels E, Ronca R, Chioldelli P, Laporte M, Vanderlinden E, Liekens S, Stevaert A, Naesens L. Influenza virus entry via the GM3 ganglioside-mediated platelet-derived growth factor receptor beta signalling pathway, *J Gen Virol*. 2019;100:583-601.
- Greenwood JR, Calkins D, Sullivan AP, Shelley JC. Towards the comprehensive, rapid, and accurate prediction of the favorable tautomeric states of drug-like molecules in aqueous solution, *Journal of computer-aided molecular design*. 2010;24:591-604.
- Shelley JC, Cholleti A, Frye LL, Greenwood JR, Timlin MR, Uchimaya M. Epik: a software program for pK(a) prediction and protonation state generation for drug-like molecules, *Journal of computer-aided molecular design*. 2007;21:681-691.
- Sastry GM, Adzhigirey M, Day T, Annabhimoju R, Sherman W. Protein and ligand preparation: parameters, protocols, and influence on virtual screening enrichments, *Journal of computer-aided molecular design*. 2013;27:221-234.

Journal Pre-proofs

39. HERG blockade obtained from protein modeling, potential energy mapping, and docking studies, *Bioorg Med Chem.* 2006;14:3160-3173.

40. Sherman W, Beard HS, Farid R. Use of an induced fit receptor structure in virtual screening, *Chem Biol Drug Des.* 2006;67:83-84.

ovel procedure for modeling ligand/receptor induced fit effects, *J Med Chem.* 2006;49:534-553.

Journal Pre-proofs



Journal Pre-proofs

Journal Pre-proofs